



Toxoplasma gondii Parasitophorous Vacuole Membrane-Associated Dense Granule Proteins Regulate Maturation of the Cyst Wall

Rebekah B. Guevara,^a Barbara A. Fox,^a David J. Bzik^a

^aDepartment of Microbiology and Immunology, The Geisel School of Medicine at Dartmouth, Lebanon, New Hampshire, USA

ABSTRACT After differentiation is triggered, the tachyzoite-stage *Toxoplasma gondii* parasitophorous vacuole membrane (PVM) has been hypothesized to transition into the cyst membrane that surrounds the cyst wall and encloses bradyzoites. Here, we tracked the localization of two PVM dense granule (GRA) proteins (GRA5 and GRA7) after *in vitro* differentiation of the tachyzoite stage parasitophorous vacuole into the mature cyst. GRA5 and GRA7 were visible at the cyst periphery at 6 h and at all later times after differentiation, suggesting that the PVM remained intact as it transitioned into the cyst membrane. By day 3 postdifferentiation, GRA5 and GRA7 were visible in a continuous pattern at the cyst periphery. In mature 7- and 10-day-old cysts permeabilized with a saponin pulse, GRA5 and GRA7 were localized to the cyst membrane and the cyst wall regions. Cysts at different stages of cyst development exhibited differential susceptibility to saponin permeabilization, and, correspondingly, saponin selectively removed GRA5 from the cyst membrane and cyst wall region in 10-day-old cysts. GRA5 and GRA7 were localized at the cyst membrane and cyst wall region at all times after differentiation of the parasitophorous vacuole, which supports a previous model proposing that the PVM develops into the cyst membrane. In addition, evaluation of $\Delta gra3$, $\Delta gra5$, $\Delta gra7$, $\Delta gra8$, and $\Delta gra14$ mutants revealed that PVM-localized GRAs were crucial to support the normal rate of accumulation of cyst wall proteins at the cyst periphery.

IMPORTANCE *Toxoplasma gondii* establishes chronic infection in humans by forming thick-walled cysts that persist in the brain. Once host immunity wanes, cysts reactivate to cause severe, and often lethal, toxoplasmic encephalitis. There is no available therapy to eliminate cysts or to prevent their reactivation. Furthermore, how the cyst membrane and cyst wall structures develop is poorly understood. Here, we visualized and tracked the localization of *Toxoplasma* parasitophorous vacuole membrane (PVM) dense granules (GRA) proteins during cyst development *in vitro*. PVM-localized GRA5 and GRA7 were found at the cyst membrane and cyst wall region throughout cyst development, suggesting that the PVM remains intact and develops into the cyst membrane. In addition, our results show that genetic deletion of PVM GRAs reduced the rate of accumulation of cyst wall cargo at the cyst periphery and suggest that PVM-localized GRAs mediate the development and maturation of the cyst wall and cyst membrane.

KEYWORDS *Toxoplasma gondii*, cysts, chronic infection, cyst wall, cyst membrane, parasitophorous vacuole membrane, dense granules, bradyzoite differentiation, cyst development, GRA

A third of the global human population is persistently infected with *Toxoplasma gondii* (1). *Toxoplasma* infection is acquired by ingestion of oocysts in water or on unwashed food, or by ingestion of tissue cysts in undercooked meat (2). While

Citation Guevara RB, Fox BA, Bzik DJ. 2020. *Toxoplasma gondii* parasitophorous vacuole membrane-associated dense granule proteins regulate maturation of the cyst wall. *mSphere* 5:e00851-19. <https://doi.org/10.1128/mSphere.00851-19>.

Editor Silvia N. J. Moreno, University of Georgia

Copyright © 2020 Guevara et al. This is an open-access article distributed under the terms of the [Creative Commons Attribution 4.0 International license](https://creativecommons.org/licenses/by/4.0/).

Address correspondence to David J. Bzik, david.j.bzik@dartmouth.edu.

 PVM GRAs build the wall. @Rebekah_Guevara

Received 15 November 2019

Accepted 19 December 2019

Published 15 January 2020

immunocompetent humans commonly control the infection, *Toxoplasma* can cause severe inflammation of the retina leading to ocular toxoplasmosis (3), and during immune suppression, cysts can reactivate in the brain causing toxoplasmic encephalitis (4, 5). The biology underlying the development of tissue cysts remains poorly understood, and current therapies do not target the cyst stage.

Tachyzoite-stage parasites actively penetrate host cells through self-driven motility, and during invagination, the parasite hijacks lipids present in the host cell plasma membrane (6) to establish an intracellular parasitophorous vacuole (PV) (7). During the process of invasion, the tachyzoite also injects bulb contents of the rhoptry organelle into the host cell cytosol (8) to form rhoptry protein (ROP)- and lipid-containing vacuoles that fuse with the nascent parasitophorous vacuole membrane (PVM) shortly after its formation (9). Within a few minutes of PV formation, the contents of the dense granules and the PVM dense granule (GRA) proteins are massively secreted into the lumen of the PV (10). These GRA proteins, together with lipids, are used to establish a nanotubular membranous intravacuolar network (IVN) in the lumen of the PV (11) that connects parasites to one another and to the PVM (12). The secreted GRA proteins can traffic to the PV space, IVN, and PVM, and a subset of GRAs are translocated past the PVM and traffic to the host cytosol or host cell nucleus (13, 14).

The PVM is a dynamic interface that supports parasite replication and survival. ROP17 (15), as well as MYR1, MYR2, and MYR3, are part of a translocon system in the PVM (16–18) that mediates the translocation of GRA16 (19, 20), GRA18 (21), GRA24 (20, 22), GRA28 (23), TgIST (24), HCE1 (25), and TEEGR (26) across the PVM. While the PVM translocation system is crucial for host cell manipulation and parasite survival (27), recent evidence suggests that after stage differentiation into bradyzoites, GRA proteins do not translocate past the cyst wall and cyst membrane, indicating either that the cyst wall is a barrier to GRA translocation or that the cyst membrane lacks a functional translocon (28). Other PVM-localized proteins, such as GRA17 and GRA23, function to facilitate the movement of small molecules or nutrients across the PVM (29, 30). A similar transport mechanism also appears to be active in the cyst stage and is mediated by a GRA17 permeability pore in the cyst membrane (31).

PVM-localized ROP5, ROP17, and ROP18 work in concert to inactivate host immunity-related GTPases (IRGs), which are part of an interferon gamma (IFN- γ)-induced mechanism that targets and eliminates foreign intracellular microbes (32–34). ROP5 prevents IRG oligomerization (35), whereas ROP17/ROP18 phosphorylate IRGs and thus disrupts their ability to attack the PV and eliminate parasites (32, 36, 37). GRA12 also resists host IFN- γ (38). IFN- γ upregulates host guanylate binding proteins (GBPs) (39–41), autophagy proteins (42, 43), and ubiquitin-associated mechanisms that target the PVM to restrict parasite replication in the PV and control infection (44–47). While macrophages harbor the most efficient IFN- γ -activated innate cell autonomous mechanisms that restrict tachyzoite replication in the PV, cysts within the central nervous system develop primarily inside neurons (48). Currently, it is unknown whether neurons can eliminate PVs or cysts via innate cell autonomous immunity or whether the cyst membrane contains parasite proteins that resist clearance mechanisms.

The hallmark of the cyst structure is a thick-walled structure, the cyst wall, that develops underneath the cyst membrane to provide a protective barrier enclosing the bradyzoites (49, 50). The major cyst wall glycoprotein, CST1, contains a mucin domain that is heavily decorated with *N*-acetylgalactosamine moieties that selectively bind to *Dolichos biflorus* agglutinin (DBA) stain (49, 51, 52). A proteomic study of purified cyst wall and cyst membrane fragments revealed the presence of many dense granule proteins in these structures (53). GRA proteins associated with the IVN (GRA2, GRA4, GRA9, and GRA12) and GRA proteins associated with the PVM (GRA3, GRA5, GRA7, GRA8, and GRA14 [10]) were identified (53). Recently, IVN GRAs were localized in the cyst wall and cyst matrix during cyst development and in mature cysts (54). Deletion of PVM- and IVN-associated GRA proteins significantly reduced cyst burdens in mice without affecting the ability of these GRA mutants to differentiate into bradyzoites and *in vitro* cysts (38, 55). In addition, the IVN GRAs (GRA2, GRA4, GRA6, GRA9, and GRA12)

were found to be important for the development and maturation of the cyst matrix and the cyst wall structures (54). Currently, the fate and role of PVM-localized GRA proteins during cyst development is unknown.

The PVM is hypothesized to develop into the cyst membrane (56). A low-CO₂ and high-pH *in vitro* tachyzoite-to-bradyzoite differentiation method (57, 58) produces mature orally infectious cysts (59) that possess the characteristic cyst structures of *in vivo* cysts isolated from brains of infected mice (60). Using this *in vitro* differentiation method, we investigated PVM GRAs (i) to track the fate of the PVM and its relationship to the development of the cyst membrane and (ii) to test whether PVM GRA proteins influence the development of the cyst wall. Our findings reveal that deletion of PVM GRAs also significantly reduced the rate of accumulation of cyst wall proteins at the cyst periphery relative to that in the cyst interior, suggesting an important role for these PVM GRA proteins in the development of the cyst wall. In addition, our results support the current model proposing that the tachyzoite-stage PVM transitions into the cyst membrane that surrounds the cyst wall.

RESULTS

DBA staining intensity at the cyst periphery relative to that in the cyst interior is decreased in mutant strains that lack expression of PVM-associated GRA proteins. GRA deletion mutants that do not express PVM-associated GRA3, GRA5, GRA7, GRA8, or GRA14 were previously developed in the low-virulence cyst-competent type II Pru Δ ku80 genetic background (38). Recently, we found that the deletion of IVN-associated GRA proteins caused a defect in the development of the cyst wall (38, 54). To determine whether a similar cyst wall defect is observed in mutants that lack expression of PVM GRAs, we measured *Dolichos biflorus* agglutinin (DBA) fluorescence intensity at the cyst peripheries of Δ gra3, Δ gra5, Δ gra7, Δ gra8, and Δ gra14 cysts (57, 58, 61, 62) (Fig. 1A). DBA selectively stains the major cyst wall protein CST1 (49, 51). DBA fluorescence intensity was quantitatively measured at the cyst periphery, which reflects CST1 cargo delivered to the cyst periphery, and was compared to that in the cyst interior, which reflects CST1 cargo not yet delivered to the cyst wall/membrane. Similar to IVN GRA deletion mutants Δ gra12 (38) and Δ gra2, Δ gra4, Δ gra6, Δ gra9 (54), the Δ gra3, Δ gra5, Δ gra7, Δ gra8, and Δ gra14 mutants exhibited a significant decrease in the DBA fluorescence intensity ratio (cyst periphery/cyst interior) (Fig. 1B).

Localization of PVM-associated GRA5 and GRA7 early after differentiation of the tachyzoite-stage PV. The cyst membrane is hypothesized to originate from the PVM (56). GRA5 localizes to the tachyzoite stage PVM and to the cyst membrane (63–67). In contrast, GRA7 associates with both the PVM and the IVN membranes in the tachyzoite-stage PV (65, 68). In mature brain cysts, GRA7 localized to membrane tubule components of the intracyst network (ICN) in the cyst matrix, a structure that resembles the IVN, as well as to convoluted membranes that were present in the cyst wall (56). We reasoned that if the cyst membrane originates from the PVM, then soon after differentiation, GRA5 and GRA7 would also localize to the cyst membrane and cyst wall compartments in the developing cyst.

We analyzed the localization of PVM-associated GRAs within the developing cyst 6 h after differentiation of the tachyzoite stage PV. Green fluorescent protein-positive (GFP⁺) bradyzoites and cyst wall proteins stained by DBA were visible within the developing cyst 6 h after differentiation (Fig. S1A-B), showing that alkaline switch differentiation rapidly upregulated expression of bradyzoite-stage genes such as LDH2 and CST1. In contrast, expression of GFP⁺ tachyzoites or DBA cyst wall proteins was not detected in the tachyzoite-stage parasitophorous vacuole (Fig. S1C). These newly differentiated cysts inside host cells were fixed in 4% paraformaldehyde, and cyst membranes were permeabilized using a pulse of saponin or using continuous saponin or Triton X-100 (Triton) detergent treatment. While DBA staining of the 6-h-old cyst was observed with both detergents, cysts were more intensely stained with DBA after permeabilization with Triton (Fig. S1A-B). In addition, consistent with the preservation

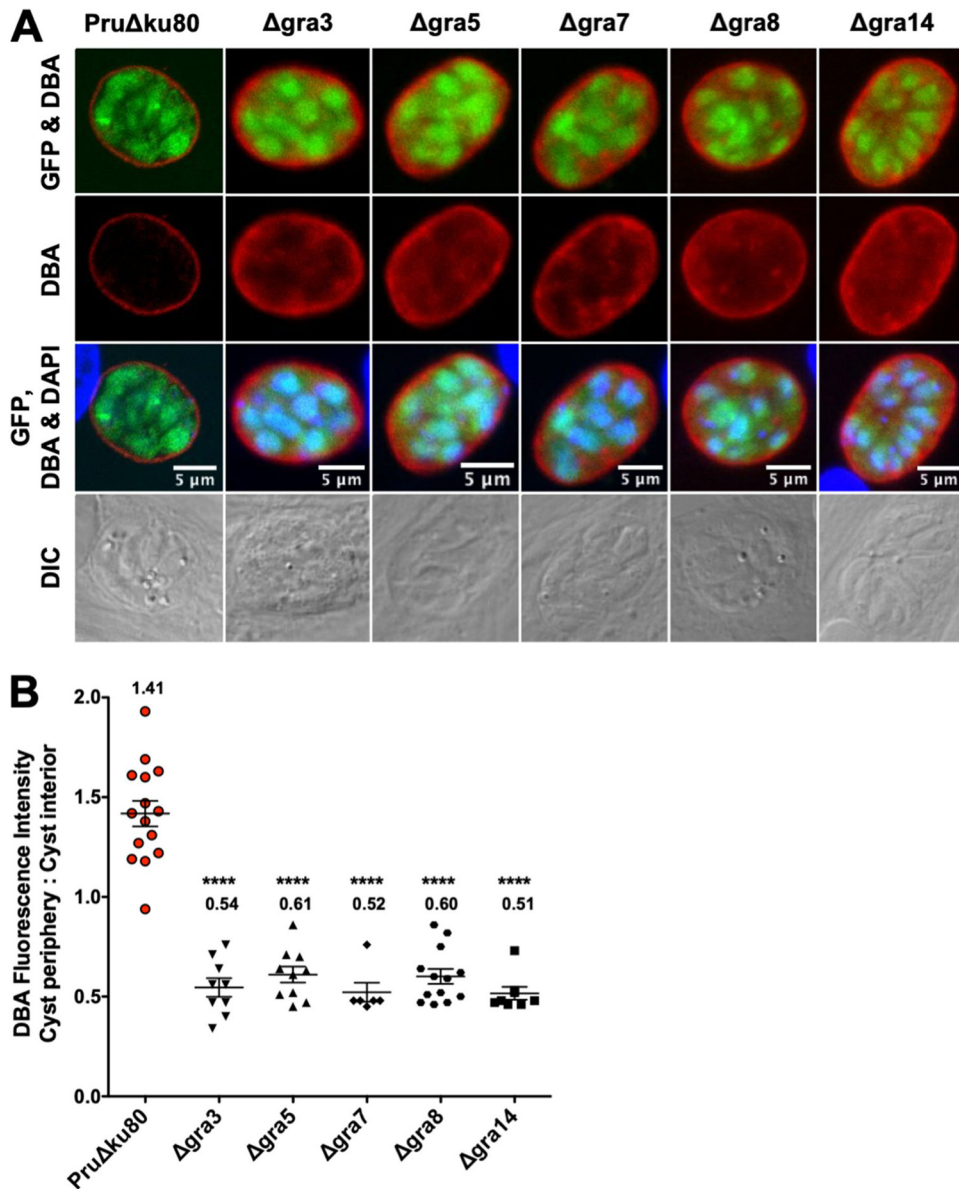


FIG 1 DBA staining intensity at the cyst periphery relative to that in the cyst interior is decreased in mutant strains that lack expression of PVM-associated GRA proteins. (A to B) *In vitro* cysts derived from different GRA deletion strains or the parental PruΔku80 strain were differentiated for 3 days. (A) Cysts were located using differential interference contrast (DIC) microscopy and imaged by confocal microscopy. The presence of bradyzoites inside cysts was verified by locating parasite nuclei with 4',6-diamidino-2-phenylindole (DAPI) staining and verifying that each parasite nucleus was surrounded by expression of cytosolic green fluorescent protein (GFP) (GFP⁺ bradyzoites). Cysts were stained with *Dolichos biflorus* agglutinin (DBA). Panels show GFP and DBA; DBA; GFP, DBA, and DAPI; and DIC. Bar, 5 μm. (B) Cysts from each strain were analyzed to determine the ratio of DBA staining intensity at the cyst periphery relative to that in the cyst interior. Data were plotted as the average ratio mean of fluorescence intensity at the cyst periphery to the cyst interior ± standard error of the mean (SEM) for each strain. Δgra3 (n = 9), Δgra5 (n = 10), Δgra7 (n = 6), Δgra8 (n = 13), Δgra14 (n = 8), and PruΔku80 (n = 15). P values were calculated with a Student's *t* test; ****, *P* < 0.0001.

of the PVM after differentiation is triggered, GRA5 (Fig. S1A) and GRA7 (Fig. S1B) were observed as bright puncta toward the cyst periphery.

Localization of GRA5 and GRA7 in immature cysts. Immature cysts were differentiated for 1, 2, or 3 days, and the localization of GRA5 (Fig. 2) and GRA7 (Fig. 3) was determined. GFP⁺ bradyzoites were visible within a DBA-stained cyst that was permeabilized with Triton. In contrast, a pulse with saponin did not permeabilize the cyst membrane of 1-, 2-, and 3-day-old cysts to visibly DBA stain the developing cyst wall

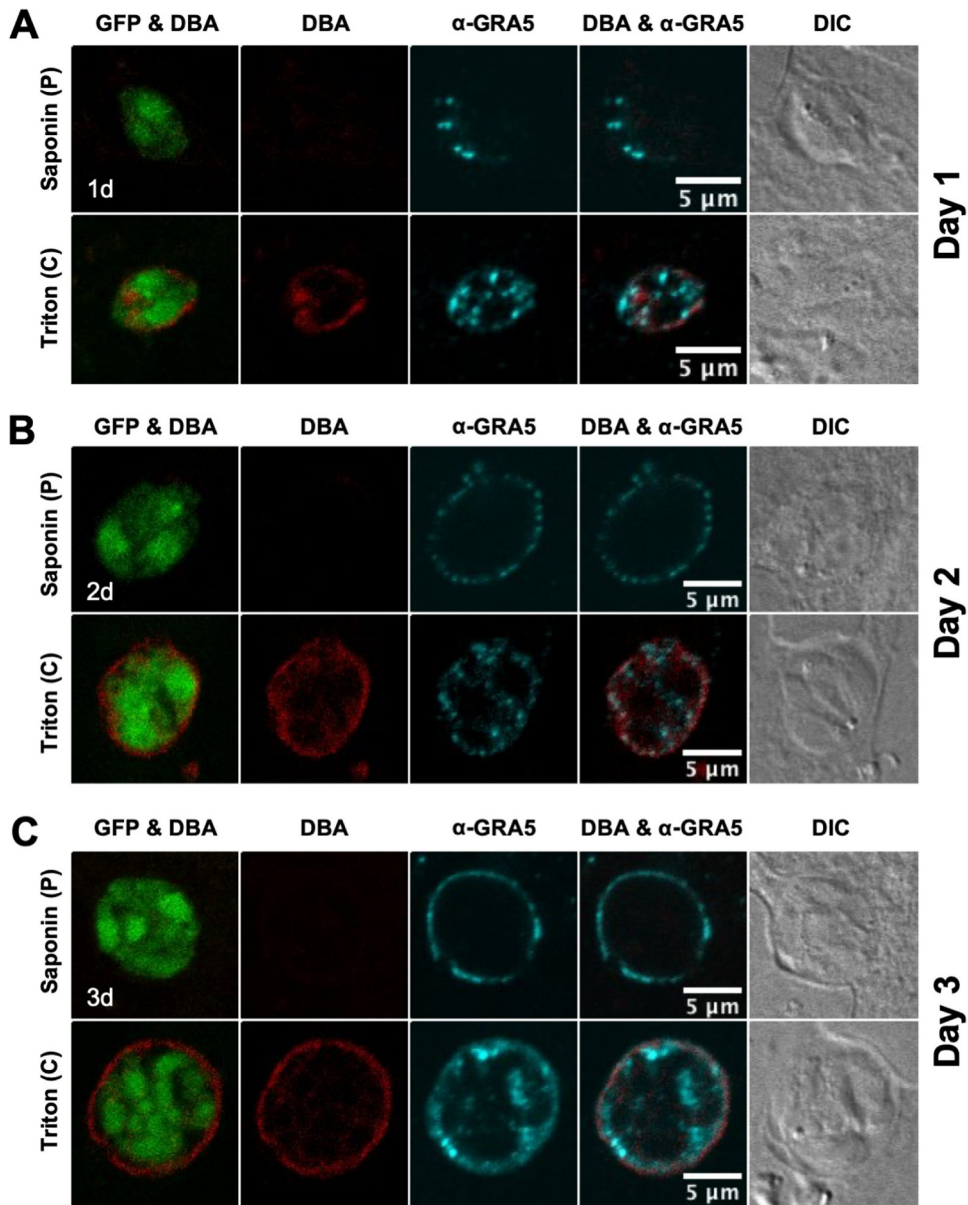


FIG 2 GRA5 localizes to the cyst periphery in immature cysts. (A to C) Infected HFFs on coverslips were treated under bradyzoite-inducing conditions to differentiate *in vitro* cysts for (A) 1 day, (B) 2 days, or (C) 3 days. Cysts were located using DIC microscopy and imaged by confocal microscopy. The presence of bradyzoites inside cysts was verified by locating parasite nuclei with DAPI staining (not shown) and verifying that each parasite nucleus was surrounded by expression of cytosolic GFP (GFP⁺ bradyzoites). Cysts fixed in 4% paraformaldehyde were permeabilized with either a short pulse (P) of saponin or with continuous (C) exposure to Triton. Cysts were stained with DBA and α -GRA5 antibody. Panels show GFP and DBA, DBA, α -GRA5, DBA and α -GRA5, and DIC. Number (*n*) of cysts analyzed, 15 to 32. Bar, 5 μ m.

(Fig. 2 and 3). However, continuous saponin permeabilization was sufficient to reveal DBA staining of the 2- and 3-day-old cyst wall with DBA (Fig. S2). Thus, compared to 6-h-old cysts (Fig. S1A-B), saponin pulse permeabilization had a reduced ability to establish detectable DBA staining of the cyst wall in 1-, 2-, and 3-day-old cysts (Fig. 2 and 3). These results revealed that the cyst wall develops underneath the cyst membrane, and suggests that the lipid composition of the 1- to 3-day-old cyst membrane is more resistant to permeabilization with saponin pulse treatment than that of cysts differentiated for 6 h.

GRA5 was localized to the cyst periphery in 1- (Fig. 2A), 2- (Fig. 2B), and 3-day-old (Fig. 2C) cysts. In contrast to a saponin pulse (Fig. 2) or continuous saponin treatment

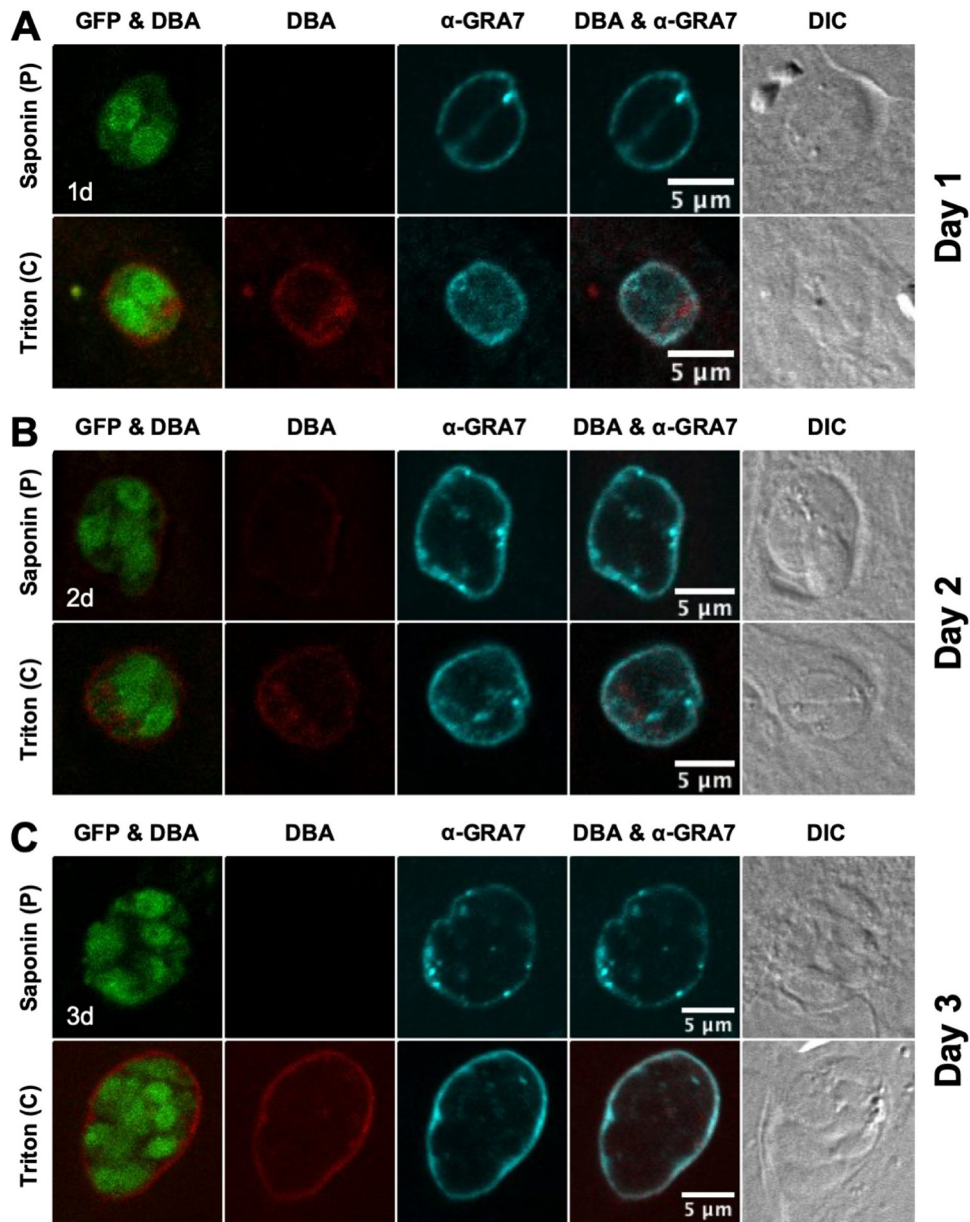


FIG 3 GRA7 localizes to the cyst periphery in immature cysts. (A to C) Infected HFFs on coverslips were treated under bradyzoite-inducing conditions to differentiate *in vitro* cysts for (A) 1 day, (B) 2 days, or (C) 3 days. Cysts were located using DIC microscopy and imaged by confocal microscopy. The presence of bradyzoites inside cysts was verified by locating parasite nuclei with DAPI staining (not shown) and verifying that each parasite nucleus was surrounded by expression of cytosolic GFP (GFP⁺ bradyzoites). Cysts fixed in 4% paraformaldehyde were permeabilized with either a short pulse (P) of saponin, or with continuous (C) exposure to Triton. Cysts were stained with DBA and α -GRA7 antibody. Panels show GFP and DBA, DBA, α -GRA7, DBA and α -GRA7, and DIC. Number (n) of cysts analyzed, 9 to 33. Bar, 5 μ m.

(Fig. S2) that localized GRA5 only at the cyst periphery, GRA5 puncta were also observed within the cyst matrix after cysts were permeabilized with Triton (Fig. 2). GRA7 was also localized at the cyst periphery of 1- (Fig. 3A), 2- (Fig. 3B), and 3-day-old (Fig. 3C) cysts. However, in comparison to GRA5 staining patterns, GRA7 puncta were rarely observed inside the cyst after permeabilization with Triton. Correspondingly, in comparison to saponin treatment, GRA5 peripheral staining was reduced after Triton treatment whereas GRA7 peripheral staining was not reduced (Fig. 2 and 3), revealing that GRA5 associated with the cyst membrane in a different manner than did GRA7. As previously reported using these permeabilization methods (54), staining of dense

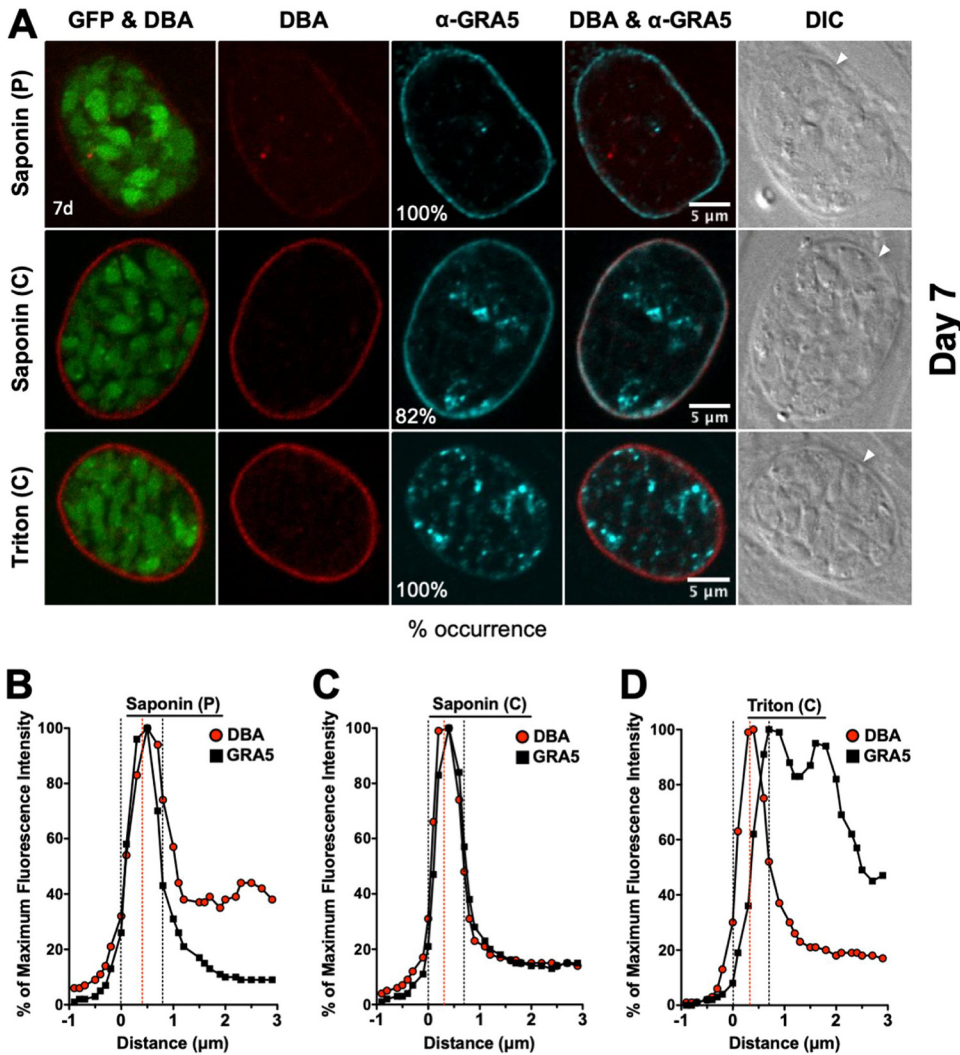


FIG 4 Localization of GRA5 in 7-day-old mature cysts. (A) Infected HFFs on coverslips were treated under bradyzoite-inducing conditions for 7 days to differentiate mature *in vitro* cysts. Cysts were located using DIC microscopy and imaged by confocal microscopy. The presence of bradyzoites inside cysts was verified by locating parasite nuclei with DAPI staining (not shown) and verifying that each parasite nucleus was surrounded by expression of cytosolic GFP (GFP⁺ bradyzoites). Cysts fixed in 4% paraformaldehyde were permeabilized with either a short pulse (P) of saponin, with continuous (C) exposure to saponin, or with continuous (C) exposure to Triton. Cysts were stained with DBA and α-GRA5 antibody. Panels show GFP and DBA, DBA, α-GRA5, DBA and α-GRA5, and DIC (cyst wall indicated by white arrow). The percent occurrence is shown for GRA5 with saponin (P) (*n* = 11; 11/11 GRA5 at the cyst membrane/wall), saponin (C) (*n* = 22; 18/22 GRA5 at the cyst membrane/wall), and Triton (*n* = 9; 9/9 GRA5 not at the cyst membrane/wall). Bar, 5 μm. (B to D) Fluorescence intensity profiles of representative cysts shown in (A) were generated to quantify the location of GRA protein(s) relative to the cyst wall, with DBA compared to α-GRA5 at day 7 for each method of permeabilization. The dotted black lines define the cyst wall region, and the dotted red line indicates the middle of the cyst wall, which corresponds to the peak DBA fluorescence intensity.

granules inside the GFP⁺ region that defines bradyzoites was not readily apparent again, indicating that this compartment was not permeabilized (Fig. 2 and 3).

Localization of GRA5 and GRA7 in mature 7-day-old cysts. GFP⁺ bradyzoites were visible in DBA-stained cysts (Fig. 4 and 5). Peripheral DBA stain was detected at the cyst wall after permeabilization with a pulse of saponin. In contrast to 1- to 3-day-old cysts, the 7-day-old cyst wall was more intensely stained with DBA after permeabilization with Triton or continuous saponin treatment (Fig. 4 and Fig. 5), indicating that increased permeabilization of the 7-day-old cyst membrane provided greater access to the cyst wall.

GRA5 was exclusively observed at the cyst periphery after permeabilization with saponin pulse (Fig. 4A). After permeabilization with continuous saponin treatment,

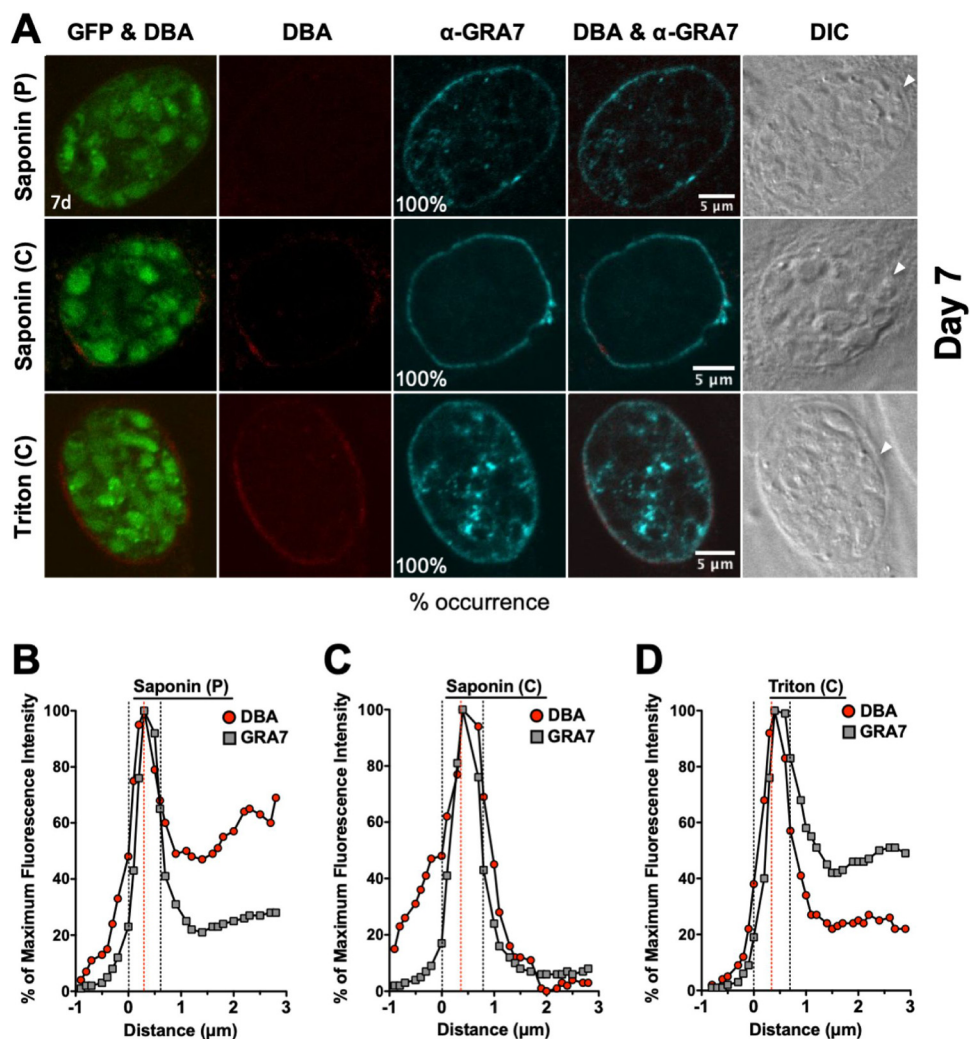


FIG 5 Localization of GRA7 in 7-day-old mature cysts. (A) Infected HFFs on coverslips were treated under bradyzoite-inducing conditions for 7 days to differentiate mature *in vitro* cysts. Cysts were located using DIC microscopy and imaged by confocal microscopy. The presence of bradyzoites inside cysts was verified by locating parasite nuclei with DAPI staining (not shown) and verifying that each parasite nucleus was surrounded by expression of cytosolic GFP (GFP⁺ bradyzoites). Cysts fixed in 4% paraformaldehyde were permeabilized with either a short pulse (P) of saponin, with continuous (C) exposure to saponin, or with continuous (C) exposure to Triton. Cysts were stained with DBA and α-GRA7 antibody. Panels show GFP and DBA, DBA, α-GRA7, DBA and α-GRA7, and DIC (cyst wall indicated by white arrow). The percent occurrence is shown for GRA7 at the cyst membrane/wall with saponin (P) ($n = 16$), saponin (C) ($n = 16$), and Triton ($n = 15$). Bar, 5 μm. (B to D) Fluorescence intensity profiles of representative cysts shown in (A) were generated to quantify the location of GRA protein(s) relative to the cyst wall, with DBA compared to α-GRA7 at day 7 for each method of permeabilization. The dotted black lines define the cyst wall region, and the dotted red line indicates the middle of the cyst wall, which corresponds to the peak DBA fluorescence intensity.

GRA5 was consistently observed at the cyst periphery and also as puncta in the cyst matrix. However, after permeabilization with Triton, GRA5 was not observed at the cyst periphery and was localized to puncta in the cyst matrix. In contrast, GRA7 was exclusively observed at the cyst periphery after permeabilization with saponin pulse or continuous saponin treatment, and GRA7 was found at the cyst periphery and in the cyst matrix after permeabilization with Triton (Fig. 5A). To quantitatively assess the location(s) of GRA5 and GRA7 in the mature 7-day-old cyst, we measured the cyst fluorescence intensity profiles for DBA and GRA5 or GRA7, respectively, using a previously reported Fiji macro (54). The cyst wall region in 7-day-old cysts occupied 6 layers (Fig. 4B to D and 5B to D). After permeabilization with a saponin pulse, the fluorescence intensity peak of GRA5 overlapped with the DBA fluorescence intensity peak and the

maximum fluorescence intensity region of GRA5 was concentrated toward the left of the DBA fluorescence intensity region (Fig. 4B), indicating that GRA5 was localized toward the exterior of the DBA stain (cyst wall) and suggesting that GRA5 is a component of the cyst membrane (Fig. 4B). However, the fluorescence intensity peak of GRA5 overlapped with the DBA fluorescence intensity peak when cysts were permeabilized with continuous saponin treatment, showing that GRA5 was present throughout the cyst wall and cyst membrane region (Fig. 4C).

In contrast to saponin permeabilization, the GRA5 fluorescence intensity peak was shifted to the right of the DBA fluorescence intensity peak after permeabilization with Triton, suggesting that GRA5 was then localized to the inner layers of the cyst wall and in the cyst matrix (Fig. 4D). In contrast to GRA5, the fluorescence intensity peak of GRA7 overlapped with the fluorescence intensity peak of DBA, confirming that GRA7 was present throughout the cyst wall and cyst membrane region after any permeabilization condition (Fig. 5B to D). These results reveal that GRA5, unlike GRA7, predominantly interacts with the cyst membrane and cyst wall in a manner that is disrupted when cysts are permeabilized with Triton.

Localization of GRA5 and GRA7 in mature 10-day-old cysts. Similar to 7-day-old cysts, DBA stain was continuously detected at the cyst wall after permeabilization with a pulse of saponin. However, DBA staining of the cyst wall was more prominent after permeabilization with Triton or continuous saponin treatment (Fig. 6 and 7). After permeabilization with a saponin pulse, GRA5 was exclusively observed at the cyst periphery (Fig. 6A), and the fluorescence intensity peak of GRA5 overlapped with the fluorescence intensity peak of DBA, indicating the presence of GRA5 in the cyst wall and cyst membrane (Fig. 6B). Compared to GRA5, GRA7 exhibited an essentially identical pattern of localization to the cyst wall and cyst membrane after permeabilization with a saponin pulse (Fig. 7A). The GRA7 fluorescence intensity peak was slightly shifted to the left of the DBA fluorescence intensity peak, suggesting that GRA7 was primarily localized in the cyst membrane and the outer layer of the cyst wall (Fig. 7B).

After permeabilization of 10-day-old cysts with continuous saponin treatment, different localization patterns of GRA5 and GRA7 were observed, which revealed differences in how GRA5 and GRA7 interacted with the cyst membrane and the cyst wall. While GRA7 was occasionally localized to puncta in the cyst matrix (Fig. 7A), the GRA7 and DBA fluorescence intensity peaks closely overlapped, revealing that GRA7 was localized in the cyst membrane and throughout the cyst wall region (Fig. 7C). In contrast, peripheral GRA5 stain was markedly reduced, and puncta of GRA5 were prominent in the cyst matrix, revealing an increased susceptibility to continuous saponin treatment (Fig. 6A). Correspondingly, GRA5 fluorescence intensity peaks were shifted to the right of the DBA fluorescence intensity peak, revealing that GRA5 was absent from the cyst membrane and was present in the inner layers of the cyst wall and in the cyst matrix (Fig. 6C).

After permeabilization of 10-day-old cysts in Triton, GRA5 and GRA7 exhibited similar patterns of localization. Peripheral GRA5 (Fig. 6A) and GRA7 (Fig. 7A) staining was reduced and prominent GRA5 and GRA7 puncta were found in the cyst matrix. Correspondingly, the GRA5 (Fig. 6D) and GRA7 (Fig. 7D) fluorescence intensity peaks were shifted to the right of the DBA fluorescence intensity peak, suggesting that GRA5 and GRA7 were absent from the cyst membrane and were localized to the inner layers of the cyst wall and in the cyst matrix.

DISCUSSION

The bradyzoite-stage cyst membrane and cyst wall structures form a barrier that maintains a chronic infection (69) and poses a therapeutic obstacle for cyst elimination (70). Our study tracked the location(s) of PVM-associated GRA5 and GRA7 from differentiation of the PV to the mature 10-day-old *in vitro* cyst. Our observations confirm a recent proteomic study of the cyst wall that identified GRA5 and GRA7 in the cyst wall of *in vitro* cysts matured for 8 days (53). Furthermore, GRA5 has been previously observed at the cyst membrane in mature cysts (63, 66). In contrast, GRA7 was

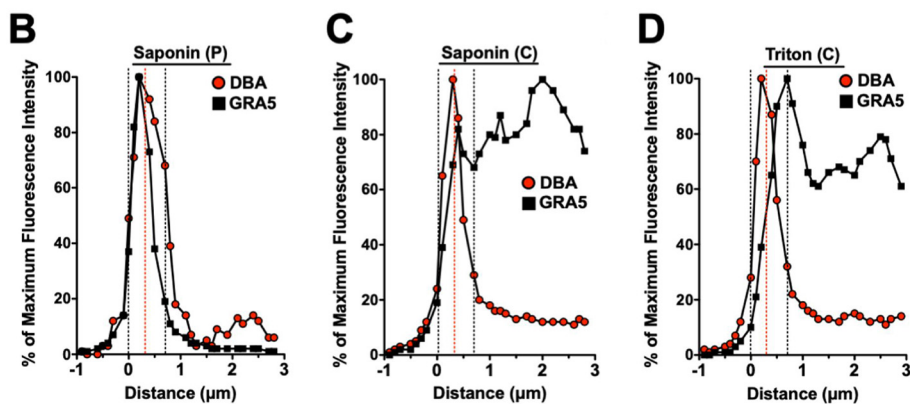
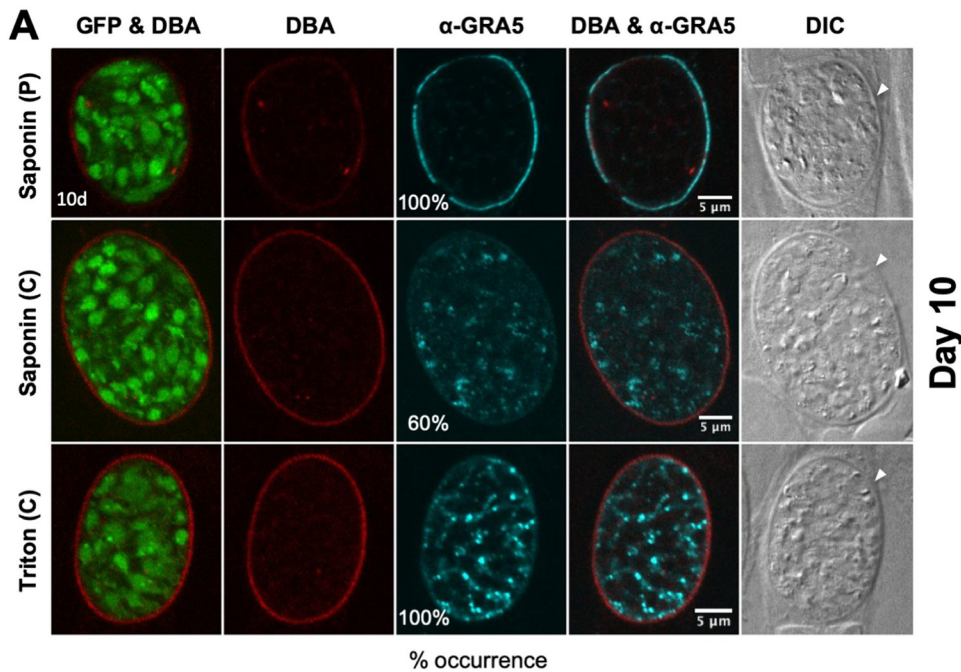


FIG 6 Localization of GRA5 in 10-day-old mature cysts. (A) Infected HFFs on coverslips were treated under bradyzoite-inducing conditions for 10 days to differentiate mature *in vitro* cysts. Cysts were located using DIC microscopy and imaged by confocal microscopy. The presence of bradyzoites inside cysts was verified by locating parasite nuclei with DAPI staining (not shown) and verifying that each parasite nucleus was surrounded by expression of cytosolic GFP (GFP⁺ bradyzoites). Cysts fixed in 4% paraformaldehyde were permeabilized with either a short pulse (P) of saponin, with continuous (C) exposure to saponin, or with continuous (C) exposure to Triton. Cysts were stained with DBA and α -GRA5 antibody. Panels show GFP and DBA, DBA, α -GRA5, DBA and α -GRA5, and DIC (cyst wall indicated by white arrow). The percent occurrence is shown for GRA5 with saponin (P) ($n = 14$; 14/14 GRA5 at the cyst membrane/wall), saponin (C) ($n = 10$; 6/10 GRA5 not at the cyst membrane/wall), and Triton (C) ($n = 11$; 11/11 GRA5 not at the cyst membrane/wall). Bar, 5 μ m. (B to D) Fluorescence intensity profiles of representative cysts shown in panel A were generated to quantify the location of GRA protein(s) relative to the cyst wall, with DBA compared to α -GRA5 at day 10 for each method of permeabilization. The dotted black lines define the cyst wall region, and the dotted red line indicates the middle of the cyst wall, which corresponds to the peak DBA fluorescence intensity.

previously localized to membrane tubule components of the intracyst network (ICN) in the cyst matrix, a structure that resembles the IVN, as well as to convoluted membranes that were present in the cyst wall (56). Our results show that after permeabilization using a saponin pulse, GRA5 and GRA7 were localized to the cyst membrane as well as to the cyst wall region. In addition, by tracking the localization of GRA5 and GRA7, our results suggest that GRA5 and GRA7 are consistently localized to the cyst membrane and cyst wall region at all times after differentiation of the tachyzoite stage PV, supporting a previous model that proposed that the PVM develops into the cyst membrane (56).

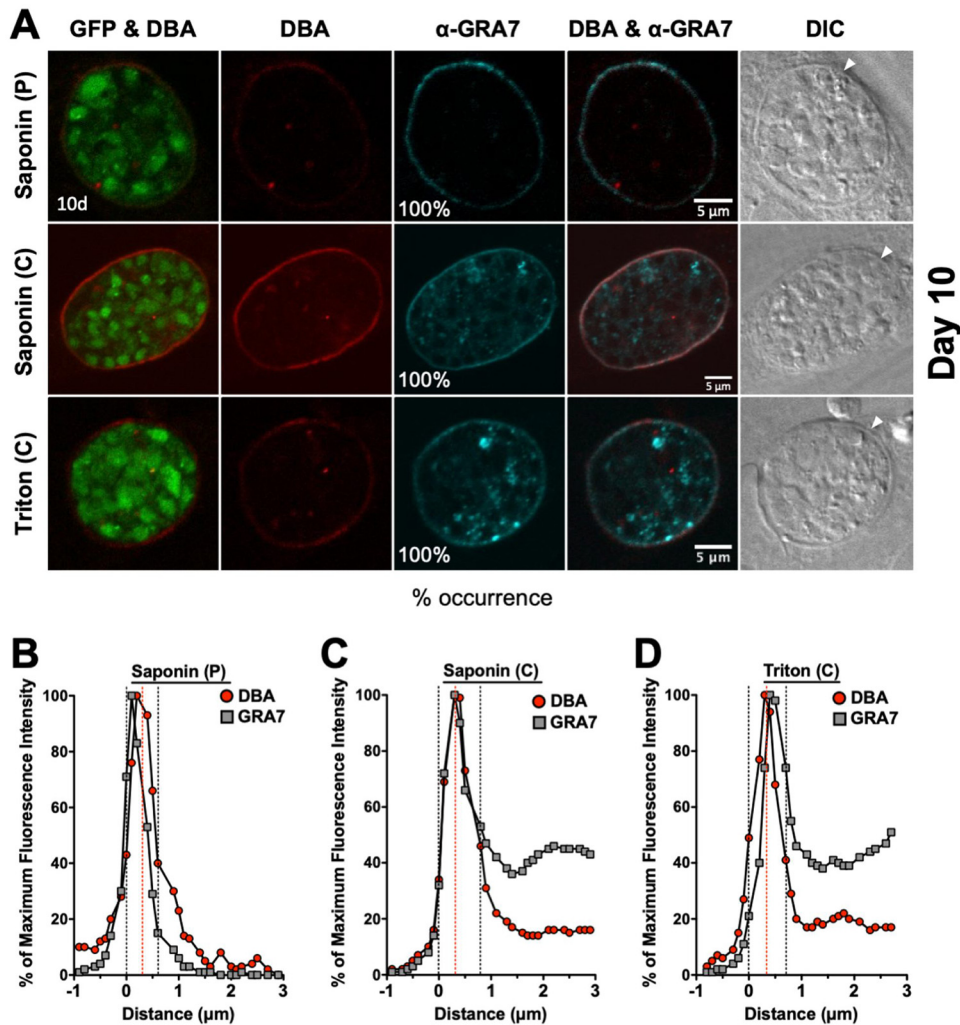


FIG 7 Localization of GRA7 in 10-day-old mature cysts. (A) Infected HFFs on coverslips were treated under bradyzoite-inducing conditions for 10 days to differentiate mature *in vitro* cysts. Cysts were located using DIC microscopy and imaged by confocal microscopy. The presence of bradyzoites inside cysts was verified by locating parasite nuclei with DAPI staining (not shown) and verifying that each parasite nucleus was surrounded by expression of cytosolic GFP (GFP⁺ bradyzoites). Cysts fixed in 4% paraformaldehyde were permeabilized with either a short pulse (P) of saponin, with continuous (C) exposure to saponin, or with continuous (C) exposure to Triton. Cysts were stained with DBA and α-GRA7 antibody. Panels show GFP and DBA, DBA, α-GRA7, DBA and α-GRA7, and DIC (cyst wall indicated by white arrow). The percent occurrence is shown for GRA7 at the cyst membrane/wall with saponin (P) ($n = 21$), saponin (C) ($n = 16$), and Triton (C) ($n = 12$). Bar, 5 μm. (B to D) Fluorescence intensity profiles of representative cysts shown in panel A were generated to quantify the location of GRA protein(s) relative to the cyst wall, with DBA compared to α-GRA7 at day 10 for each method of permeabilization. The dotted black lines define the cyst wall region, and the dotted red line indicates the middle of the cyst wall, which corresponds to the peak DBA fluorescence intensity.

Measurement of DBA stain localization in $\Delta gra3$, $\Delta gra5$, $\Delta gra7$, $\Delta gra8$, and $\Delta gra14$ *in vitro* cysts revealed that PVM GRAs were crucial to support the normal rate of accumulation of cyst wall proteins at the cyst periphery. These results mirror recent results we reported for IVN $\Delta gra12$ (38), and $\Delta gra2$, $\Delta gra4$, $\Delta gra6$, and $\Delta gra9$ *in vitro* cysts (54) and suggest that both IVN- and PVM-localized GRAs are crucial for the development and the maturation of the cyst wall and cyst membrane. These findings support the hypothesis that membranes at the cyst periphery are occupied by GRA proteins that play key roles in the development and maturation of the cyst wall and cyst membrane. The functions of some of the PVM GRAs have been reported in the tachyzoite-stage PV. GRA3 is a type I transmembrane protein that localizes to the PVM and IVN (71), and GRA3 molecules were observed at the cyst wall (56). GRA3 interacts with calcium-

modulating ligand (CAMLG), a type II transmembrane protein of ER (72), and it recruits and engulfs host Golgi into the PV (73). GRA5 is a type I transmembrane protein that is targeted to the PVM (64). GRA5 molecules are concentrated at the cyst periphery (67) and associate with the cyst membrane (63, 66). GRA7 is a transmembrane protein that localizes to the PVM, IVN (74), and membranous PV extensions (PVE) that extend from the PVM into the host cytosol (68). GRA7 molecules associate with ROP2 and ROP4 (75) and interact with ROP5/ROP18 complex at the PVM to regulate the ROP18-specific inactivation of Irga6 to resist IFN- γ -activated host cell innate immunity (76). GRA7 acts as a garroting protein that sequesters host endolysosomes within the tachyzoite-stage PV (77). GRA7 tubulates artificial liposomes, and targeted deletion of GRA7 under serum-deprived conditions leads to slow tachyzoite-stage parasite growth (77). GRA7 molecules were observed in association with membranes in the cyst wall and the cyst matrix (56). GRA8 is a proline-rich protein that localizes to the PVM (78) and is a component of the subpellicular cytoskeleton in tachyzoite-stage parasites (79). GRA14 is a transmembrane protein that localizes to the PVM, IVN, and PVE (80). GRA14 can be transferred between PVs via PVEs (80). Deletion of GRA3 (81), GRA7, GRA8, and GRA14 did not affect the parasite's ability to differentiate *in vitro* but markedly reduced cyst burden *in vivo* (38). However, the specific role(s) of these PVM GRA molecules in the cyst wall and cyst membrane during cyst development still remains to be determined.

Intriguingly, depletion of low-density lipoprotein (LDL)-derived cholesterol increases tachyzoite-to-bradyzoite stage conversion (82). Our findings show that the cyst membrane of immature cysts was differentially permeabilized by saponin and Triton X-100 (Triton) detergent treatments. Saponin selectively interacts with cholesterol in the lipid bilayer membrane, causing the formation of permeability holes (83). In contrast, Triton is a nonionic detergent that inserts into membranes to dissolve lipid-lipid and lipid-protein interactions, while typically preserving protein-protein interactions (84). In immature cysts 3 days old or younger, DBA staining of the cyst wall was more intense after permeabilization in Triton in comparison to saponin pulse. However, this difference was not observed in mature 7- or 10-day-old cysts, and DBA staining of the cyst wall was equivalent with both detergents. In addition, DBA staining intensity varied at different times of cyst development after permeabilization using a saponin pulse. DBA staining of 6-h-old cysts was apparent. In contrast, DBA staining of immature 1-, 2-, and 3-day-old cysts was not detected. However, in 7- and 10-day-old mature cysts, the cyst wall was DBA stained after saponin pulse permeabilization. These DBA staining patterns of the cyst wall after saponin pulse permeabilization suggest that the lipid composition of the cyst membrane, and perhaps those of other membranes present in the cyst wall, such as the ICN membranes (56), varies during cyst development. Detection of DBA staining in 6-h-old cysts but not in 1-, 2-, or 3-day-old cysts suggests that the cholesterol content of the cyst membrane may decrease between 6- and 24-h postdifferentiation. If so, this would mirror the fate of cholesterol in the PVM after tachyzoite invasion, which is highest in the newly formed PVM and is markedly reduced in the old PVM after several rounds of tachyzoite replication have occurred (85). The higher cholesterol content of the early PVM appears to arise via an invasion mechanism involving the formation of cholesterol-rich vacuoles that fuse to the nascent PVM (85–87). In addition, after immature cysts developed into mature 7- and 10-day-old cysts, the cyst membranes became more saponin sensitive and exhibited increased DBA staining of the cyst wall after saponin pulse permeabilization. The increased saponin sensitivity of the cyst membranes in mature cysts is consistent with the ability of 3- and 7-day-old *in vitro* cysts to contain more cholesterol-containing lipid droplets derived from the host cell (88). Thus, while it is tempting to speculate that the cholesterol content of the cyst membrane increases as cyst mature, other interpretations of these results are possible, and future experiments are necessary to measure the cholesterol content in cyst membranes during cyst development.

The glycosylated cyst wall forms beneath the cyst membrane. How cyst wall cargo is delivered to the cyst periphery remains unknown. A favored hypothesis is that wall cargo is delivered in vesicles secreted by bradyzoite-stage parasites. Our data revealed

bright puncta of GRA5 and GRA7 close to the cyst periphery at 6 h after differentiation. This phenotype is similar to previous findings that GRA1, GRA2, GRA4, GRA6, GRA9, and GRA12 were observed in puncta at the cyst periphery 6 h after differentiation (54). It is tempting to speculate that these puncta represent secreted vesicles; however, future electron or high-resolution microscopy studies are needed to investigate the mechanisms that direct the delivery of cyst wall cargo to the developing cyst wall.

To assess the proximity of PVM GRAs, we used a previously developed quantitative method (54), which defined the cyst wall region to allow the fluorescence intensity of GRA5 and GRA7 in relation to the DBA-stained cyst wall to be measured.

The initial PVM is hypothesized to undergo changes that culminates in a limiting cyst membrane. Cyst wall proteins congregate at the cyst periphery (54), presumably underneath the cyst membrane, to develop the cyst wall. The mature cyst membrane has been observed to be noncontinuous (ruffled) and is present in the outer layers of the cyst wall (49, 53, 56). The cyst wall structure has two recognizable layers, a densely compacted outer layer and a less densely compacted inner layer that faces the cyst matrix (56). Using these cyst membrane and cyst wall descriptions in conjunction with our cyst wall analysis, we localized GRA5 and GRA7 in the cyst membrane since their fluorescence intensity peaks were observed outside and exterior to the DBA-stained cyst wall fluorescence intensity peak. In addition, GRA5 and GRA7 were localized throughout the cyst wall, suggesting that GRA5 and GRA7 also associate with the ICN membranes that penetrate into the cyst wall from the cyst matrix (56).

When mature 7- or 10-day-old cysts were permeabilized with Triton, GRA5 and GRA7 were localized in the inner layers of the cyst wall and in the cyst matrix as prominent puncta. Remarkably, saponin permeabilization caused differential localization of GRA5 and GRA7 selectively in 10-day-old mature cysts. GRA5 was localized to the inner layers of the cyst wall and to prominent puncta in the cyst matrix after continuous saponin permeabilization. In contrast, GRA7 was localized at the cyst membrane and cyst wall region. The simplest explanation for this differential localization is that GRA5 most likely resides in cholesterol-rich lipid rafts in the cyst membrane, whereas GRA7 does not. Alternatively, GRA7 may interact with a protein component of the cyst wall that stabilizes its cyst membrane localization after saponin permeabilization, but, as mentioned earlier, not after Triton permeabilization. Elucidating the functions of PVM GRAs during cyst development is necessary to define the mechanisms that regulate the development and maturation of the cyst wall and cyst membrane.

MATERIALS AND METHODS

Culture conditions and strains. Type II Prugniaud (Pru) background *Toxoplasma gondii* parasites were maintained *in vitro* by serial passage of tachyzoites in human foreskin fibroblast (HFF) monolayers (ATCC SCRS-1041.1) cultured in Eagle's modified essential medium (EMEM; Lonza) containing 1% fetal bovine serum (FBS; Life Technologies), 2 mM glutamine, 100 units/ml penicillin, and 100 μ g/ml streptomycin at 36°C in 95% air and 5% CO₂. HFF cells were maintained in EMEM, 10% FBS (HyClone), 2 mM glutamine, 100 units/ml penicillin, and 100 μ g/ml streptomycin at 37°C in 95% air and 5% CO₂. The parental Pru strain Pru Δ ku80 was previously made transgenic for green fluorescent protein (GFP) under the control of the LDH2 bradyzoite stage-specific promoter (89). Strains used in this study were developed using the Δ ku80 knockout strain of the type II Pru strain using previously described methods (38, 90).

***In vitro* cyst differentiation assay.** Tachyzoites were differentiated *in vitro* into bradyzoites within cysts essentially as previously and elegantly described by Knoll and colleagues (57). Differentiation medium contained Roswell Park Memorial Institute medium (RPMI) without bicarbonate supplemented with 2.05 mM L-glutamine (HyClone), 20 mM HEPES-free acid (IBI Scientific), 1% XL-glutamine (a long-lasting stable form of glutamine; VWR), 1% FBS, and 1% penicillin-streptomycin. The pH of differentiation medium was adjusted to 8.1 with sodium hydroxide and filter sterilized. HFF cells were cultured on circular micro cover glass until confluent (Electron Microscopy Sciences), and confluent monolayers were infected with type II Pru parasites at a multiplicity of infection (MOI) of ~0.5. Infected cells were washed 3 h after infection once in Dulbecco's phosphate-buffered saline (DPBS) supplemented with Ca²⁺ and Mg²⁺ and incubated in differentiation medium for 6 h, 1 day, 2 days, 3 days, 7 days, or 10 days at 37°C in ambient air. Medium was changed on days 3 and 7.

Cyst immunofluorescence assay and cyst locating. Infected cells were fixed in 4% paraformaldehyde for 10 min, and the excess was quenched with 0.1 M glycine. Infected cells were permeabilized and blocked in either (i) 0.01% saponin (Sigma) for 10 min, (ii) 3%FBS/0.01% saponin for 30 min at room temperature (RT), with this permeabilization solution used throughout the experiment, or (iii) 3%FBS/

0.2% Triton X-100 for 30 min at RT, with this permeabilization solution used throughout the experiment. All samples were incubated with a 1:1,000 dilution of primary mouse monoclonal α -GRA5 antibody (63) or with a 1:1,000 dilution of primary rabbit α -GRA7 (91) (antibodies purchased from Biotem [Apprieu, France] or kindly provided by D. Jacobs, Innogenetics-Fujire-bio Europe N.V. [Ghent, Belgium]). Preparations were washed three times with DPBS supplemented with Ca^{2+} and Mg^{2+} and incubated for 1 h at RT with a 1:1,000 dilution of secondary goat anti-rabbit (H+L) (Thermo Fisher) and goat anti-mouse IgG (H+L) antibodies conjugated to Alexa Fluor 647 (Cell Signaling). All samples were incubated with a 1:250 dilution of rhodamine-labeled *Dolichos biflorus* agglutinin (Vector Laboratories) for 1 h at RT. The Pru background used in this study has a bradyzoite-specific gene, LDH2, under a GFP promoter (89), which is expressed when the parasites switch from tachyzoites to bradyzoites. Samples were mounted in SlowFade Gold antifade with 4',6-diamidino-2-phenylindole (DAPI; Life Technologies) and then imaged with a Nikon A1Rsi confocal microscope (Nikon, Inc.) using an Apo TIRF 100 \times oil differential interference contrast (DIC) N20 objective. Cysts were randomly selected for analysis by locating cysts using DIC microscopy. Bradyzoite differentiation in cysts was confirmed by GFP⁺ bradyzoites. The focal plane (from a z-stack) selected for quantification was from the middle of the cyst, where the cyst size is maximal. Raw .nd2 files of cyst images were imported into Fiji for processing. Images were minimally processed for brightness (image \rightarrow adjust \rightarrow color balance) in Fiji (92). The number of cysts for each strain analyzed in each experiment is shown in the figure legends for Fig. 1 to 7 and Supplemental Fig. S1 and S2. The percent occurrence was calculated as the number of cysts showing the representative phenotype that are shown in the representative image out of the total number of cysts imaged.

Cyst fluorescence intensity profiles. Raw .nd2 image files were imported into Fiji to measure fluorescence intensity parallel to the cyst wall as previously described (54). Images were cropped to isolate each cyst. A macro was written to generate a reliable mask of the cyst, slightly outside the cyst wall, using the DBA-rhodamine channel. The DBA-rhodamine channel was used to threshold the cyst, and holes were filled inside to get a continuous mask of the whole cyst. Successive layers were generated based on the original mask, growing or shrinking using the “dilate” or “erode” morphological operations. Layers were generally 1 pixel thick. The fluorescence intensity of each region was measured for a selected fluorescent channel, DBA, GRA5, or GRA7. The macro generated layers within the cyst until the minimum area of the (shrinking) layer reached 1,000 pixels². Layers were created by dilation to measure the fluorescence intensity outside the cyst, which provided the background fluorescence intensity. All data were imported into Excel to be further analyzed, as previously described (54). Calculated percentage of maximum fluorescence intensity and distance (μm) values were imported and graphed in Prism.

Cyst wall definition and analysis. The cyst wall region was identified and defined as previously described (54). The cyst wall outer region was identified by DBA, while the inner region was determined by GFP, which identifies the parasites within the cyst. The cyst wall region is defined by outer and inner boundaries, which were determined by the first point less than 50% of maximum fluorescence intensity of DBA and GFP, respectively. The cyst wall region is marked by dotted black lines, and the peak of DBA fluorescence is marked by a dotted red line. Next, we evaluated location of GRA5 or GRA7 in comparison to the DBA-stained cyst wall using fluorescence intensity measured at the same time within the cyst. This cyst wall analysis was used to determine if two proteins were observed in the same layer.

Cyst total fluorescence intensity quantification assay. Raw .nd2 image files were imported into Fiji to measure total fluorescence intensity at the cyst periphery and within the cyst interior, as previously described (54). The cyst periphery was determined to be the cyst wall plus two layers, which were added to include proteins near the cyst wall but not yet incorporated into the cyst wall. Fluorescence for DBA was measured in $\Delta ku80$, $\Delta gra3$, $\Delta gra5$, $\Delta gra7$, $\Delta gra8$, and $\Delta gra14$ strains. To measure background fluorescence, a circle was drawn using the freehand selection tool, and fluorescence was measured outside the cyst on three different sides. All data were imported into Excel to be further analyzed as previously described (54). All ratios were entered and graphed in Prism. A ratio of <1 means there is greater DBA fluorescence intensity in the cyst interior compared to that in the cyst periphery, a ratio of 1 represents an equal DBA fluorescence intensity at the cyst periphery to that in the cyst interior, and a ratio of >1 means there is greater DBA fluorescence intensity at the cyst periphery than in the cyst interior. *P* values were calculated with a Student's *t* test; ****, $P < 0.0001$.

Immunofluorescence assay for tachyzoites. HFFs were cultured on circular micro cover glass and were infected with parasites for 24 h. Samples were fixed in 4% paraformaldehyde for 10 min, permeabilized with 0.01% saponin (Sigma) for 10 min, and blocked with 10% FBS for 20 min. All samples were incubated with a 1:250 dilution of rhodamine-labeled *Dolichos biflorus* agglutinin (Vector Laboratories) for 1 h at RT. All samples were mounted in SlowFade Gold antifade with DAPI (Life Technologies) and imaged at $\times 100$ with a Nikon A1Rsi confocal microscope (Nikon, Inc.). Vacuoles were located using differential interference contrast (DIC) microscopy. Confocal images as raw .nd2 files were imported and minimally processed for brightness in Fiji (92).

Statistical analysis. Unpaired *t* tests were used to calculate *P* values. All calculations of average, plus or minus standard error of the mean (SEM), and *P* values were performed using GraphPad Prism software version 5.0c.

SUPPLEMENTAL MATERIAL

Supplemental material is available online only.

FIG S1, TIF file, 0.3 MB.

FIG S2, TIF file, 0.1 MB.

ACKNOWLEDGMENTS

We are grateful to Zdenek Svindrych for writing the Fiji macro used for quantification of cyst images acquired using confocal microscopy, and the BioMT Core imaging facility for training and advice. We thank D. Jacobs (Innogenetics-Fujire-bio Europe N.V., Ghent, Belgium) for sharing antibody used in this study.

This work was supported by National Institutes of Health (NIH) grants AI105563, AI108489, AI131630, and AI137118 to D.J.B. R.B.G. was a trainee on NIH grants T32AI007519, and T32AI007363. The BioMT Core (imaging core facility) was supported by the National Institutes of General Medical Science (NIGMS) (grant P20GM113132).

R.B.G., B.A.F., and D.B.J. conceptualized the experiments. R.B.G. performed the experiments and analyzed the data. All authors contributed to writing, reviewing, and editing the manuscript.

REFERENCES

- Flegr J, Prandota J, Sovickova M, Israili ZH. 2014. Toxoplasmosis—a global threat. Correlation of latent toxoplasmosis with specific disease burden in a set of 88 countries. *PLoS One* 9:e90203. <https://doi.org/10.1371/journal.pone.0090203>.
- Tenter AM, Heckeroth AR, Weiss LM. 2000. *Toxoplasma gondii*: from animals to humans. *Int J Parasitol* 30:1217–1258. [https://doi.org/10.1016/s0020-7519\(00\)00124-7](https://doi.org/10.1016/s0020-7519(00)00124-7).
- Park YH, Nam HW. 2013. Clinical features and treatment of ocular toxoplasmosis. *Korean J Parasitol* 51:393–399. <https://doi.org/10.3347/kjp.2013.51.4.393>.
- Luft BJ, Remington JS. 1992. Toxoplasmic encephalitis in AIDS. *Clin Infect Dis* 15:211–222. <https://doi.org/10.1093/clinids/15.2.211>.
- Weiss LM, Dubey JP. 2009. Toxoplasmosis: a history of clinical observations. *Int J Parasitol* 39:895–901. <https://doi.org/10.1016/j.ijpara.2009.02.004>.
- Suss-Toby E, Zimmerberg J, Ward GE. 1996. *Toxoplasma* invasion: the parasitophorous vacuole is formed from host cell plasma membrane and pinches off via a fission pore. *Proc Natl Acad Sci U S A* 93:8413–8418. <https://doi.org/10.1073/pnas.93.16.8413>.
- Sibley LD. 2004. Intracellular parasite invasion strategies. *Science* 304:248–253. <https://doi.org/10.1126/science.1094717>.
- Boothroyd JC, Dubremetz JF. 2008. Kiss and spit: the dual roles of *Toxoplasma rhoptries*. *Nat Rev Microbiol* 6:79–88. <https://doi.org/10.1038/nrmicro1800>.
- Hakansson S, Charron AJ, Sibley LD. 2001. *Toxoplasma* evacuoles: a two-step process of secretion and fusion forms the parasitophorous vacuole. *EMBO J* 20:3132–3144. <https://doi.org/10.1093/emboj/20.12.3132>.
- Mercier C, Cesbron-Delauw MF. 2015. *Toxoplasma* secretory granules: one population or more? *Trends Parasitol* 31:60–71. <https://doi.org/10.1016/j.pt.2014.12.002>.
- Travier L, Mondragon R, Dubremetz JF, Musset K, Mondragon M, Gonzalez S, Cesbron-Delauw MF, Mercier C. 2008. Functional domains of the *Toxoplasma* GRA2 protein in the formation of the membranous nanotubular network of the parasitophorous vacuole. *Int J Parasitol* 38:757–773. <https://doi.org/10.1016/j.ijpara.2007.10.010>.
- Mercier C, Dubremetz JF, Rauscher B, Lecordier L, Sibley LD, Cesbron-Delauw MF. 2002. Biogenesis of nanotubular network in *Toxoplasma* parasitophorous vacuole induced by parasite proteins. *Mol Biol Cell* 13:2397–2409. <https://doi.org/10.1091/mbc.e02-01-0021>.
- Lerliche MA, Dubremetz JF. 1990. Exocytosis of *Toxoplasma gondii* dense granules into the parasitophorous vacuole after host cell invasion. *Parasitol Res* 76:559–562. <https://doi.org/10.1007/bf00932560>.
- Dubremetz JF, Achbarou A, Bermudes D, Joiner KA. 1993. Kinetics and pattern of organelle exocytosis during *Toxoplasma gondii*/host-cell interaction. *Parasitol Res* 79:402–408. <https://doi.org/10.1007/bf00931830>.
- Panas MW, Ferrel A, Naor A, Tenborg E, Lorenzi HA, Boothroyd JC, Panas MW, Ferrel A, Naor A, Tenborg E, Lorenzi HA, Boothroyd JC. 2019. Translocation of dense granule effectors across the parasitophorous vacuole membrane in *Toxoplasma*-infected cells requires the activity of ROP17, a rhoptry protein kinase. *mSphere* 4:e00276-19. <https://doi.org/10.1128/mSphere.00276-19>.
- Naor A, Panas MW, Marino N, Coffey MJ, Tonkin CJ, Boothroyd JC, Naor A, Panas MW, Marino N, Coffey MJ, Tonkin CJ, Boothroyd JC. 2018. MYR1-dependent effectors are the major drivers of a host cell's early response to *Toxoplasma*, including counteracting MYR1-independent effects. *mBio* 9:e02401-17. <https://doi.org/10.1128/mBio.02401-17>.
- Franco M, Panas MW, Marino ND, Lee MC, Buchholz KR, Kelly FD, Bednarski JJ, Sleckman BP, Pourmand N, Boothroyd JC. 2016. A novel secreted protein, MYR1, is central to *Toxoplasma*'s manipulation of host cells. *mBio* 7:e02231-15. <https://doi.org/10.1128/mBio.02231-15>.
- Marino ND, Panas MW, Franco M, Theisen TC, Naor A, Rastogi S, Buchholz KR, Lorenzi HA, Boothroyd JC. 2018. Identification of a novel protein complex essential for effector translocation across the parasitophorous vacuole membrane of *Toxoplasma gondii*. *PLoS Pathog* 14:e1006828. <https://doi.org/10.1371/journal.ppat.1006828>.
- Bougourd A, Durandau E, Brenier-Pinchart MP, Ortet P, Barakat M, Kieffer S, Curt-Varesano A, Curt-Bertini RL, Bastien O, Coute Y, Pelloux H, Hakimi MA. 2013. Host cell subversion by *Toxoplasma* GRA16, an exported dense granule protein that targets the host cell nucleus and alters gene expression. *Cell Host Microbe* 13:489–500. <https://doi.org/10.1016/j.chom.2013.03.002>.
- Curt-Varesano A, Braun L, Ranquet C, Hakimi MA, Bougdour A. 2016. The aspartyl protease TgASP5 mediates the export of the *Toxoplasma* GRA16 and GRA24 effectors into host cells. *Cell Microbiol* 18:151–167. <https://doi.org/10.1111/cmi.12498>.
- He H, Brenier-Pinchart M-P, Braun L, Kraut A, Touquet B, Couté Y, Tardieux I, Hakimi M-A, Bougdour A, He H, Brenier-Pinchart M-P, Braun L, Kraut A, Touquet B, Couté Y, Tardieux I, Hakimi M-A, Bougdour A. 2018. Characterization of a *Toxoplasma* effector uncovers an alternative GSK3/beta-catenin-regulatory pathway of inflammation. *Elife* 7:e39887. <https://doi.org/10.7554/eLife.39887>.
- Braun L, Brenier-Pinchart MP, Yogavel M, Curt-Varesano A, Curt-Bertini RL, Hussain T, Kieffer-Jaquinod S, Coute Y, Pelloux H, Tardieux I, Sharma A, Belhali H, Bougdour A, Hakimi MA. 2013. A *Toxoplasma* dense granule protein, GRA24, modulates the early immune response to infection by promoting a direct and sustained host p38 MAPK activation. *J Exp Med* 210:2071–2086. <https://doi.org/10.1084/jem.20130103>.
- Nadipuram SM, Kim EW, Vashisht AA, Lin AH, Bell HN, Coppens I, Wohlschlegel JA, Bradley PJ, Nadipuram SM, Kim EW, Vashisht AA, Lin AH, Bell HN, Coppens I, Wohlschlegel JA, Bradley PJ. 2016. *In vivo* biotinylation of the *Toxoplasma* parasitophorous vacuole reveals novel dense granule proteins important for parasite growth and pathogenesis. *mBio* 7:e00808-16. <https://doi.org/10.1128/mBio.00808-16>.
- Gay G, Braun L, Brenier-Pinchart MP, Vollaire J, Josserand V, Bertini RL, Varesano A, Touquet B, De Bock PJ, Coute Y, Tardieux I, Bougdour A, Hakimi MA. 2016. *Toxoplasma gondii* TgIST co-opts host chromatin repressors dampening STAT1-dependent gene regulation and IFN-gamma-mediated host defenses. *J Exp Med* 213:1779–1798. <https://doi.org/10.1084/jem.20160340>.
- Panas MW, Naor A, Cygan AM, Boothroyd JC, Panas MW, Naor A, Cygan AM, Boothroyd JC. 2019. *Toxoplasma* controls host cyclin E expression through the use of a novel MYR1-dependent effector protein, HCE1. *mBio* 10:e00674-19. <https://doi.org/10.1128/mBio.00674-19>.
- Braun L, Brenier-Pinchart M-P, Hammoudi P-M, Cannella D, Kieffer-Jaquinod S, Vollaire J, Josserand V, Touquet B, Couté Y, Tardieux I, Bougdour A, Hakimi M-A. 2019. The *Toxoplasma* effector TEEGR promotes parasite persistence by modulating NF-kappaB signalling via

- EZH2. *Nat Microbiol* 4:1208–1220. <https://doi.org/10.1038/s41564-019-0431-8>.
27. Hakimi MA, Olias P, Sibley LD. 2017. *Toxoplasma* effectors targeting host signaling and transcription. *Clin Microbiol Rev* 30:615–645. <https://doi.org/10.1128/CMR.00005-17>.
 28. Krishnamurthy S, Saeij J. 2018. *Toxoplasma* does not secrete the GRA16 and GRA24 effectors beyond the parasitophorous vacuole membrane of tissue cysts. *Front Cell Infect Microbiol* 8:366. <https://doi.org/10.3389/fcimb.2018.00366>.
 29. Gold DA, Kaplan AD, Lis A, Bett GC, Rosowski EE, Cirelli KM, Bougdour A, Sidik SM, Beck JR, Lourido S, Egea PF, Bradley PJ, Hakimi MA, Rasmusson RL, Saeij JP. 2015. The *Toxoplasma* dense granule proteins GRA17 and GRA23 mediate the movement of small molecules between the host and the parasitophorous vacuole. *Cell Host Microbe* 17:642–652. <https://doi.org/10.1016/j.chom.2015.04.003>.
 30. Schwab JC, Beckers CJ, Joiner KA. 1994. The parasitophorous vacuole membrane surrounding intracellular *Toxoplasma gondii* functions as a molecular sieve. *Proc Natl Acad Sci U S A* 91:509–513. <https://doi.org/10.1073/pnas.91.2.509>.
 31. Paredes-Santos T, Wang Y, Waldman B, Lourido S, Saeij JP. 2019. The GRA17 parasitophorous vacuole membrane permeability pore contributes to bradyzoite viability. *Front Cell Infect Microbiol* 9:321. <https://doi.org/10.3389/fcimb.2019.00321>.
 32. Etheridge RD, Alagunan A, Tang K, Lou HJ, Turk BE, Sibley LD. 2014. The *Toxoplasma* pseudokinase ROP5 forms complexes with ROP18 and ROP17 kinases that synergize to control acute virulence in mice. *Cell Host Microbe* 15:537–550. <https://doi.org/10.1016/j.chom.2014.04.002>.
 33. Fleckenstein MC, Reese ML, Konen-Waisman S, Boothroyd JC, Howard JC, Steinfield T. 2012. A *Toxoplasma gondii* pseudokinase inhibits host IRG resistance proteins. *PLoS Biol* 10:e1001358. <https://doi.org/10.1371/journal.pbio.1001358>.
 34. Behnke MS, Fentress SJ, Mashayekhi M, Li LX, Taylor GA, Sibley LD. 2012. The polymorphic pseudokinase ROP5 controls virulence in *Toxoplasma gondii* by regulating the active kinase ROP18. *PLoS Pathog* 8:e1002992. <https://doi.org/10.1371/journal.ppat.1002992>.
 35. Reese ML, Shah N, Boothroyd JC. 2014. The *Toxoplasma* pseudokinase ROP5 is an allosteric inhibitor of the immunity-related GTPases. *J Biol Chem* 289:27849–27858. <https://doi.org/10.1074/jbc.M114.567057>.
 36. Steinfield T, Konen-Waisman S, Tong L, Pawlowski N, Lamkemeyer T, Sibley LD, Hunn JP, Howard JC. 2010. Phosphorylation of mouse immunity-related GTPase (IRG) resistance proteins is an evasion strategy for virulent *Toxoplasma gondii*. *PLoS Biol* 8:e1000576. <https://doi.org/10.1371/journal.pbio.1000576>.
 37. Fentress SJ, Behnke MS, Dunay IR, Mashayekhi M, Rommereim LM, Fox BA, Bzik DJ, Taylor GA, Turk BE, Lichti CF, Townsend RR, Qiu W, Hui R, Beatty WL, Sibley LD. 2010. Phosphorylation of immunity-related GTPases by a *Toxoplasma gondii*-secreted kinase promotes macrophage survival and virulence. *Cell Host Microbe* 8:484–495. <https://doi.org/10.1016/j.chom.2010.11.005>.
 38. Fox BA, Guevara RB, Rommereim LM, Falla A, Bellini V, Pêtre G, Rak C, Cantillana V, Dubremetz J-F, Cesbron-Delauw M-F, Taylor GA, Mercier C, Bzik DJ, Fox BA, Guevara RB, Rommereim LM, Falla A, Bellini V, Pêtre G, Rak C, Cantillana V, Dubremetz J-F, Cesbron-Delauw M-F, Taylor GA, Mercier C, Bzik DJ. 2019. *Toxoplasma gondii* parasitophorous vacuole membrane-associated dense granule proteins orchestrate chronic infection and GRA12 underpins resistance to host IFN- γ . *mBio* 10:e00589-19. <https://doi.org/10.1128/mBio.00589-19>.
 39. Degrandi D, Kravets E, Konermann C, Beuter-Gunia C, Klumpers V, Lahme S, Wischmann E, Mausberg AK, Beer-Hammer S, Pfeffer K. 2013. Murine guanylate binding protein 2 (mGBP2) controls *Toxoplasma gondii* replication. *Proc Natl Acad Sci U S A* 110:294–299. <https://doi.org/10.1073/pnas.1205635110>.
 40. Selleck EM, Fentress SJ, Beatty WL, Degrandi D, Pfeffer K, Virgin HW, Macmicking JD, Sibley LD. 2013. Guanylate-binding protein 1 (Gbp1) contributes to cell-autonomous immunity against *Toxoplasma gondii*. *PLoS Pathog* 9:e1003320. <https://doi.org/10.1371/journal.ppat.1003320>.
 41. Kravets E, Degrandi D, Ma Q, Peulen T-O, Klumpers V, Felekyan S, Kühnemuth R, Weidtkamp-Peters S, Seidel CA, Pfeffer K, Kravets E, Degrandi D, Ma Q, Peulen T-O, Klumpers V, Felekyan S, Kühnemuth R, Weidtkamp-Peters S, Seidel CA, Pfeffer K. 2016. Guanylate binding proteins directly attack *Toxoplasma gondii* via supramolecular complexes. *Elife* 5:e11479. <https://doi.org/10.7554/eLife.11479>.
 42. Haldar AK, Piro AS, Pilla DM, Yamamoto M, Coers J. 2014. The E2-like conjugation enzyme Atg3 promotes binding of IRG and Gbp proteins to *Chlamydia*- and *Toxoplasma*-containing vacuoles and host resistance. *PLoS One* 9:e86684. <https://doi.org/10.1371/journal.pone.0086684>.
 43. Gupta SL, Carlin JM, Pyati P, Dai W, Pfefferkorn ER, Murphy MJ. 1994. Antiparasitic and antiproliferative effects of indoleamine 2,3-dioxygenase enzyme expression in human fibroblasts. *Infect Immun* 62:2277–2284.
 44. Foltz C, Napolitano A, Khan R, Clough B, Hirst EM, Frickel EM. 2017. TRIM21 is critical for survival of *Toxoplasma gondii* infection and localises to GBP-positive parasite vacuoles. *Sci Rep* 7:5209. <https://doi.org/10.1038/s41598-017-05487-7>.
 45. Clough B, Wright JD, Pereira PM, Hirst EM, Johnston AC, Henriques R, Frickel EM. 2016. K63-linked ubiquitination targets *Toxoplasma gondii* for endo-lysosomal destruction in IFN γ -stimulated human cells. *PLoS Pathog* 12:e1006027. <https://doi.org/10.1371/journal.ppat.1006027>.
 46. Haldar AK, Foltz C, Finethy R, Piro AS, Feeley EM, Pilla-Moffett DM, Komatsu M, Frickel EM, Coers J. 2015. Ubiquitin systems mark pathogen-containing vacuoles as targets for host defense by guanylate binding proteins. *Proc Natl Acad Sci U S A* 112:E5628–37. <https://doi.org/10.1073/pnas.1515966112>.
 47. Selleck EM, Orchard RC, Lassen KG, Beatty WL, Xavier RJ, Levine B, Virgin HW, Sibley LD. 2015. A noncanonical autophagy pathway restricts *Toxoplasma gondii* growth in a strain-specific manner in IFN- γ -activated human cells. *mBio* 6:e01157-15. <https://doi.org/10.1128/mBio.01157-15>.
 48. Cabral CM, Tuladhar S, Dietrich HK, Nguyen E, MacDonald WR, Trivedi T, Devineni A, Koshy AA. 2016. Neurons are the primary target cell for the brain-tropic intracellular parasite *Toxoplasma gondii*. *PLoS Pathog* 12:e1005447. <https://doi.org/10.1371/journal.ppat.1005447>.
 49. Tomita T, Bzik DJ, Ma YF, Fox BA, Markillie LM, Taylor RC, Kim K, Weiss LM. 2013. The *Toxoplasma gondii* cyst wall protein CST1 is critical for cyst wall integrity and promotes bradyzoite persistence. *PLoS Pathog* 9:e1003823. <https://doi.org/10.1371/journal.ppat.1003823>.
 50. Ferguson DJ, Hutchison WM. 1987. An ultrastructural study of the early development and tissue cyst formation of *Toxoplasma gondii* in the brains of mice. *Parasitol Res* 73:483–491. <https://doi.org/10.1007/bf00535321>.
 51. Zhang YW, Halonen SK, Ma YF, Wittner M, Weiss LM. 2001. Initial characterization of CST1, a *Toxoplasma gondii* cyst wall glycoprotein. *Infect Immun* 69:501–507. <https://doi.org/10.1128/IAI.69.1.501-507.2001>.
 52. Tomita T, Sugi T, Yakubu R, Tu V, Ma Y, Weiss LM, Tomita T, Sugi T, Yakubu R, Tu V, Ma Y, Weiss LM. 2017. Making home sweet and sturdy: *Toxoplasma gondii* ppGalNAC-Ts glycosylate in hierarchical order and confer cyst wall rigidity. *mBio* 8:e02048-16. <https://doi.org/10.1128/mBio.02048-16>.
 53. Tu V, Mayoral J, Sugi T, Tomita T, Han B, Ma YF, Weiss LM, Tu V, Mayoral J, Sugi T, Tomita T, Han B, Ma YF, Weiss LM. 2019. Enrichment and proteomic characterization of the cyst wall from *in vitro* *Toxoplasma gondii* cysts. *mBio* 10:e00469-19. <https://doi.org/10.1128/mBio.00469-19>.
 54. Guevara RB, Fox BA, Falla A, Bzik DJ, Guevara RB, Fox BA, Falla A, Bzik DJ. 2019. *Toxoplasma gondii* intravacuolar-network-associated dense granule proteins regulate maturation of the cyst matrix and cyst wall. *mSphere* 4:e00487-19. <https://doi.org/10.1128/mSphere.00487-19>.
 55. Fox BA, Falla A, Rommereim LM, Tomita T, Giggley JP, Mercier C, Cesbron-Delauw MF, Weiss LM, Bzik DJ. 2011. Type II *Toxoplasma gondii* KU80 knockout strains enable functional analysis of genes required for cyst development and latent infection. *Eukaryot Cell* 10:1193–1206. <https://doi.org/10.1128/EC.00297-10>.
 56. Lemgruber L, Lupetti P, Martins-Duarte ES, De Souza W, Vommaro RC. 2011. The organization of the wall filaments and characterization of the matrix structures of *Toxoplasma gondii* cyst form. *Cell Microbiol* 13:1920–1932. <https://doi.org/10.1111/j.1462-5822.2011.01681.x>.
 57. Tobin C, Pollard A, Knoll L. 2010. *Toxoplasma gondii* cyst wall formation in activated bone marrow-derived macrophages and bradyzoite conditions. *J Vis Exp* (42):e2091. <https://doi.org/10.3791/2091>.
 58. Weiss LM, Laplace D, Takvorian PM, Cali A, Tanowitz HB, Wittner M. 1994. Development of bradyzoites of *Toxoplasma gondii* in vitro. *J Eukaryot Microbiol* 41:185.
 59. Fux B, Nawas J, Khan A, Gill DB, Su C, Sibley LD. 2007. *Toxoplasma gondii* strains defective in oral transmission are also defective in developmental stage differentiation. *Infect Immun* 75:2580–2590. <https://doi.org/10.1128/IAI.00085-07>.
 60. Sahn M, Fischer HG, Gross U, Reiter-Owona I, Seitz HM. 1997. Cyst formation by *Toxoplasma gondii* in vivo and in brain-cell culture: a comparative morphology and immunocytochemistry study. *Parasitol Res* 83:659–665. <https://doi.org/10.1007/s004360050315>.

61. Matrajt M, Donald RG, Singh U, Roos DS. 2002. Identification and characterization of differentiation mutants in the protozoan parasite *Toxoplasma gondii*. *Mol Microbiol* 44:735–747. <https://doi.org/10.1046/j.1365-2958.2002.02904.x>.
62. Weiss LM, Laplace D, Takvorian PM, Tanowitz HB, Cali A, Wittner M. 1995. A cell culture system for study of the development of *Toxoplasma gondii* bradyzoites. *J Eukaryot Microbiol* 42:150–157. <https://doi.org/10.1111/j.1550-7408.1995.tb01556.x>.
63. Torpier G, Charif H, Darcy F, Liu J, Darde ML, Capron A. 1993. *Toxoplasma gondii*: differential location of antigens secreted from encysted bradyzoites. *Exp Parasitol* 77:13–22. <https://doi.org/10.1006/expr.1993.1056>.
64. Lecordier L, Mercier C, Sibley LD, Cesbron-Delauw MF. 1999. Transmembrane insertion of the *Toxoplasma gondii* GRA5 protein occurs after soluble secretion into the host cell. *Mol Biol Cell* 10:1277–1287. <https://doi.org/10.1091/mbc.10.4.1277>.
65. Lecordier L, Mercier C, Torpier G, Tourvieille B, Darcy F, Liu JL, Maes P, Tartar A, Capron A, Cesbron-Delauw MF. 1993. Molecular structure of a *Toxoplasma gondii* dense granule antigen (GRA 5) associated with the parasitophorous vacuole membrane. *Mol Biochem Parasitol* 59:143–153. [https://doi.org/10.1016/0166-6851\(93\)90015-p](https://doi.org/10.1016/0166-6851(93)90015-p).
66. Ferguson DJ. 2004. Use of molecular and ultrastructural markers to evaluate stage conversion of *Toxoplasma gondii* in both the intermediate and definitive host. *Int J Parasitol* 34:347–360. <https://doi.org/10.1016/j.ijpara.2003.11.024>.
67. Lane A, Soete M, Dubremetz JF, Smith JE. 1996. *Toxoplasma gondii*: appearance of specific markers during the development of tissue cysts in vitro. *Parasitol Res* 82:340–346. <https://doi.org/10.1007/s004360050123>.
68. Jacobs D, Dubremetz JF, Loyens A, Bosman F, Saman E. 1998. Identification and heterologous expression of a new dense granule protein (GRA7) from *Toxoplasma gondii*. *Mol Biochem Parasitol* 91:237–249. [https://doi.org/10.1016/s0166-6851\(97\)00204-1](https://doi.org/10.1016/s0166-6851(97)00204-1).
69. Soete M, Fortier B, Camus D, Dubremetz JF. 1993. *Toxoplasma gondii*: kinetics of bradyzoite-tachyzoite interconversion in vitro. *Exp Parasitol* 76:259–264. <https://doi.org/10.1006/expr.1993.1031>.
70. Frenkel JK. 1956. Pathogenesis of toxoplasmosis and of infections with organisms resembling *Toxoplasma*. *Ann N Y Acad Sci* 64:215–251. <https://doi.org/10.1111/j.1749-6632.1956.tb36616.x>.
71. Henriquez FL, Nickdel MB, McLeod R, Lyons RE, Lyons K, Dubremetz JF, Grigg ME, Samuel BU, Roberts CV. 2005. *Toxoplasma gondii* dense granule protein 3 (GRA3) is a type I transmembrane protein that possesses a cytoplasmic dilysine (KKXX) endoplasmic reticulum (ER) retrieval motif. *Parasitology* 131:169–179. <https://doi.org/10.1017/s0031182005007559>.
72. Kim JY, Ahn HJ, Ryu KJ, Nam HW. 2008. Interaction between parasitophorous vacuolar membrane-associated GRA3 and calcium modulating ligand of host cell endoplasmic reticulum in the parasitism of *Toxoplasma gondii*. *Korean J Parasitol* 46:209–216. <https://doi.org/10.3347/kjp.2008.46.4.209>.
73. Deffieu MS, Alayi TD, Slomianny C, Tomavo S. 2019. The *Toxoplasma gondii* dense granule protein TgGRA3 interacts with host Golgi and dysregulates anterograde transport. *Biol Open* 8:bio039818. <https://doi.org/10.1242/bio.039818>.
74. Fischer HG, Stachelhaus S, Sahn M, Meyer HE, Reichmann G. 1998. GRA7, an excretory 29 kDa *Toxoplasma gondii* dense granule antigen released by infected host cells. *Mol Biochem Parasitol* 91:251–262. [https://doi.org/10.1016/s0166-6851\(97\)00227-2](https://doi.org/10.1016/s0166-6851(97)00227-2).
75. Dunn JD, Ravindran S, Kim SK, Boothroyd JC. 2008. The *Toxoplasma gondii* dense granule protein GRA7 is phosphorylated upon invasion and forms an unexpected association with the rhoptry proteins ROP2 and ROP4. *Infect Immun* 76:5853–5861. <https://doi.org/10.1128/IAI.01667-07>.
76. Hermanns T, Muller UB, Konen-Waisman S, Howard JC, Steinfeldt T. 2016. The *Toxoplasma gondii* rhoptry protein ROP18 is an Irga6-specific kinase and regulated by the dense granule protein GRA7. *Cell Microbiol* 18:244–259. <https://doi.org/10.1111/cmi.12499>.
77. Coppens I, Dunn JD, Romano JD, Pypaert M, Zhang H, Boothroyd JC, Joiner KA. 2006. *Toxoplasma gondii* sequesters lysosomes from mammalian hosts in the vacuolar space. *Cell* 125:261–274. <https://doi.org/10.1016/j.cell.2006.01.056>.
78. Carey KL, Donahue CG, Ward GE. 2000. Identification and molecular characterization of GRA8, a novel, proline-rich, dense granule protein of *Toxoplasma gondii*. *Mol Biochem Parasitol* 105:25–37. [https://doi.org/10.1016/s0166-6851\(99\)00160-7](https://doi.org/10.1016/s0166-6851(99)00160-7).
79. Díaz-Martín RD, Mercier C, Gómez de León CT, González RM, Pozos SG, Ríos-Castro E, García RA, Fox BA, Bzik DJ, Flores RM. 2019. The dense granule protein 8 (GRA8) is a component of the sub-pellicular cytoskeleton in *Toxoplasma gondii*. *Parasitol Res* 118:1899–1918. <https://doi.org/10.1007/s00436-019-06298-7>.
80. Rome ME, Beck JR, Turetzky JM, Webster P, Bradley PJ. 2008. Intervacuolar transport and unique topology of GRA14, a novel dense granule protein in *Toxoplasma gondii*. *Infect Immun* 76:4865–4875. <https://doi.org/10.1128/IAI.00782-08>.
81. Craver MP, Knoll LJ. 2007. Increased efficiency of homologous recombination in *Toxoplasma gondii* dense granule protein 3 demonstrates that GRA3 is not necessary in cell culture but does contribute to virulence. *Mol Biochem Parasitol* 153:149–157. <https://doi.org/10.1016/j.molbiopara.2007.02.013>.
82. Ihara F, Nishikawa Y. 2014. Starvation of low-density lipoprotein-derived cholesterol induces bradyzoite conversion in *Toxoplasma gondii*. *Parasit Vectors* 7:248. <https://doi.org/10.1186/1756-3305-7-248>.
83. Seeman P, Cheng D, Iles GH. 1973. Structure of membrane holes in osmotic and saponin hemolysis. *J Cell Biol* 56:519–527. <https://doi.org/10.1083/jcb.56.2.519>.
84. Bhairi SM. 2001. Detergents: a guide to the properties and uses of detergents in biological systems. Calbiochem-Novabiochem Corporation, San Diego, CA.
85. Coppens I, Joiner KA. 2003. Host but not parasite cholesterol controls *Toxoplasma* cell entry by modulating organelle discharge. *Mol Biol Cell* 14:3804–3820. <https://doi.org/10.1091/mbc.e02-12-0830>.
86. Besteiro S, Bertrand-Michel J, Lebrun M, Vial H, Dubremetz JF. 2008. Lipidomic analysis of *Toxoplasma gondii* tachyzoites rhoptries: further insights into the role of cholesterol. *Biochem J* 415:87–96. <https://doi.org/10.1042/BJ20080795>.
87. Tahara M, Andrabi SB, Matsubara R, Aonuma H, Nagamune K. 2016. A host cell membrane microdomain is a critical factor for organelle discharge by *Toxoplasma gondii*. *Parasitol Int* 65:378–388. <https://doi.org/10.1016/j.parint.2016.05.012>.
88. Nolan SJ, Romano JD, Kline JT, Coppens I, Nolan SJ, Romano JD, Kline JT, Coppens I. 2018. Novel approaches to kill *Toxoplasma gondii* by exploiting the uncontrolled uptake of unsaturated fatty acids and vulnerability to lipid storage inhibition of the parasite. *Antimicrob Agents Chemother* 62:e00347–18. <https://doi.org/10.1128/AAC.00347-18>.
89. Singh U, Brewer JL, Boothroyd JC. 2002. Genetic analysis of tachyzoite to bradyzoite differentiation mutants in *Toxoplasma gondii* reveals a hierarchy of gene induction. *Mol Microbiol* 44:721–733. <https://doi.org/10.1046/j.1365-2958.2002.02903.x>.
90. Fox BA, Ristuccia JG, Giggley JP, Bzik DJ. 2009. Efficient gene replacements in *Toxoplasma gondii* strains deficient for nonhomologous end joining. *Eukaryot Cell* 8:520–529. <https://doi.org/10.1128/EC.00357-08>.
91. Saavedra R, De Meuter F, Héron P. 1990. Monoclonal antibodies identify new *Toxoplasma gondii* soluble antigens. *Hybridoma* 9:453–463. <https://doi.org/10.1089/hyb.1990.9.453>.
92. Schindelin J, Arganda-Carreras I, Frise E, Kaynig V, Longair M, Pietzsch T, Preibisch S, Rueden C, Saalfeld S, Schmid B, Tinevez JY, White DJ, Hartenstein V, Eliceiri K, Tomancak P, Cardona A. 2012. Fiji: an open-source platform for biological-image analysis. *Nat Methods* 9:676–682. <https://doi.org/10.1038/nmeth.2019>.